Modified diabolo antennas for broadband enhancement of sub-terahertz oscillating magnetic fields

Ohmichi, Eiji

Takigawa, Ryoto

Igo, Yuma

Ohta, Hitoshi

(Citation)
Optics Express,32(13):22331-22339

(Issue Date)
2024-06-17

(Resource Type)
journal article

(Version)
Version of Record

Research Article | Vol. 32, No. 13 / 17 Jun 2024 / Optics Express 22331
Optics EXPRESS

Modified diabolo antennas for broadband enhancement of sub-terahertz oscillating magnetic fields

EIJI OHMICHI,[1,*] RYOTO TAKIGAWA,[1] YUMA IGO,[1] AND HITOSHI OHTA[1,2]

[1]Graduate School of Science, Kobe University, 1-1 Rokkodai, Nada, Kobe 657-8501, Japan
[2]Molecular Photoscience Research Center, Kobe University, 1-1 Rokkodai, Nada, Kobe 657-8501, Japan
[*]ohmichi@harbor.kobe-u.ac.jp

Abstract: Enhancement of the magnetic field components of electromagnetic waves is of particular interest across a wide range of applications such as enhanced magnetic dipole emission and increased sensitivity of magnetic resonance. Diabolo antennas are known to significantly enhance the local intensity of oscillating magnetic fields. Although the enhancement factor is sufficiently high for these purposes, the drawback is a narrow frequency band due to their resonant nature. Here we propose modified diabolo antennas, or nested U-shaped antennas, to expand the working frequency band in the sub-terahertz region. In this study, we investigated the geometrical dependence of nested U-shaped antennas and optimized their shape for practical applications in sub-terahertz electron spin resonance spectroscopy.

1. Introduction

Metallic planar antennas are widely used in a vast array of applications from microwave [1] to infrared [2] and optical [3] regions. In sensing applications, these antennas not only enhance the local intensity of electromagnetic waves but also strongly modify the interactions between them and materials of interest. One well-known example in the optical region is bow-tie antennas [4–6], in which oscillating electric fields are confined within the sub-wavelength volume between the antenna gap, and are strongly enhanced by significant factors exceeding 10^3. A similar example is metallic nanoparticles [7,8], in which oscillating electric fields are strongly enhanced by surface plasmon resonance. This effect has been applied to nano-scale spectroscopy using tip-enhanced interactions [9,10] and single molecular sensing in nanoparticle-attached whispering gallery mode resonators [11,12]. It is noted that these applications are based on the enhancement of electric field components of the incident electromagnetic waves.

On the other hand, metallic antennas to enhance the local oscillating magnetic fields have not been popular because of the minor effects of their magnetic interactions. Proposed applications include enhanced dipole emission [13,14] and increased sensitivity of magnetic resonance [15,16]. In the latter case, the transition probability between different spin states is proportional to the square of oscillating magnetic field components, so the sensitivity would be greatly improved by introducing antennas to enhance the magnetic field components. This idea can be applied to high-frequency electron spin resonance (ESR). It has been shown that ESR in the sub-terahertz (THz) region is useful to investigate magnetic resonance modes of magnetic samples. Particularly, antiferromagnets, which have recently attracted much attention from the viewpoint of high-speed and high-density spintronics devices [17,18], often exhibit antiferromagnetic (AF) magnon modes in the sub-THz region [19]. However, detection of such AF modes is not straightforward because of the low power of the light source and the absence of a cavity in such a high-frequency region. So, the enhancement of oscillating magnetic fields is strongly desired to improve the sensitivity of high-frequency ESR.

#525006 https://doi.org/10.1364/OE.525006
Journal © 2024 Received 27 Mar 2024; revised 20 May 2024; accepted 26 May 2024; published 3 Jun 2024

Optics EXPRESS

A diabolo antenna is a kind of planar metallic antenna that significantly enhances oscillating magnetic fields [20]. Shown in Fig. 1(a) is a typical shape of diabolo antenna, in which a pair of triangular fins are connected by a thin strip. When linearly polarized electromagnetic waves are irradiated normal to the antenna, circularly oscillating magnetic fields are induced around the strip by the oscillating current flowing in the strip. A lot of diabolo antenna designs have been reported to enhance oscillating magnetic fields in the optical regions [21,22]. However, from the viewpoint of ESR spectroscopy, standard diabolo antennas only work in a narrow frequency band because of their resonant nature and are not suitable for spectroscopic purposes in their present form. Thus, broadband enhancement of the magnetic components is strongly required for ESR spectroscopy in the sub-THz region. For this purpose, we modeled a modified type of diabolo antenna, a nested U-shaped antenna, in this study. We found that its working frequency band becomes wider and can be tuned flexibly by changing the geometrical parameters. In addition, nested U-shaped antennas can be made more compact than standard diabolo antennas, and it would be useful to produce strong local oscillating fields at the sample position to improve the sensitivity of high-frequency ESR spectroscopy.

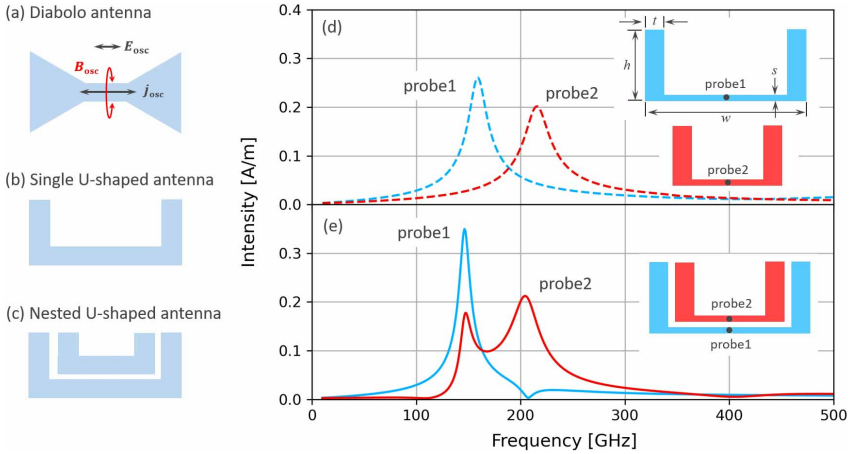

Fig. 1. (a) Standard diabolo antenna, (b) single U-shaped antenna and (c) nested U-shaped antenna. The working principle of the diabolo antenna is also shown in (a). Frequency responses of (d) small and large single U-shaped antennas and (e) their nested U-shaped antenna, respectively. The insets show the corresponding shapes of the antennas and the positions of their probes for their respective antennas.

2. Simulation

In this study, the CST Studio suite was used to obtain all simulation results. To simulate the frequency response of the proposed antenna structures, the frequency-domain solver based on the finite element method was used. The minimum mesh size and the maximum mesh number were typically $\lambda/2000 \sim \lambda/3000$ and 3×10^6, respectively, where λ is the wavelength of incident beams. The accuracy of the solver calculation was set to 1×10^{-4}. Simulation parameters were routinely checked if the simulated results were physically sound. The antenna and substrate materials in this work were aluminum and single-crystal silicon, respectively, which were chosen by considering the practical fabrication process. A series of antenna structures with different geometrical parameters was modeled on the silicon substrate, and linearly polarized plane waves were irradiated normal to the antenna. The influence of non-uniform incident beams was found to be small because the lateral antenna size (typically 0.2λ-0.3λ) was much smaller than the focused beam spot size (see Supplement 1). The polarization direction was parallel to the thin

Optics EXPRESS

strip of the antenna. The amplitude of the incident electric field was fixed at E=1 V/m. This value corresponds to the oscillating magnetic field amplitude of $H=E/Z=2.7\times10^{-3}$ A/m, where Z is the vacuum impedance. The horizontal components of the oscillating magnetic fields were monitored at typically 10 nm above the strip surface. In the practical setup of ESR spectroscopy, a sample is placed on the strip and a static magnetic field is applied perpendicular to the antenna. Thus, the oscillating magnetic field at the sample position is orthogonal to the external field, and the prerequisite for magnetic dipole transition is satisfied.

3. Results and discussion

To begin with, we consider a single U-shaped antenna, as shown in Fig.1 (b), which is regarded as the half-cut diabolo antenna shown in Fig. 1(a). Here we consider two types of single U-shaped antennas with different geometrical parameters: w=419μm, h=171μm, t=52μm and s=15 μm, and w=285μm, h=141μm, t=52μm and s=15 μm, where w is the antenna width, h is the antenna height, t is the fin width, and s is the strip width. The antenna thickness was fixed at 140 nm. It was confirmed that the variation of the antenna thickness has little influence on the antenna properties. A probe port to monitor the horizontal component of the oscillating magnetic field is placed at the center of the thin strip. Figure 1(d) shows the frequency dependence of the horizontal oscillating magnetic field of the respective single U-shaped antennas. Enhancement of the horizontal components on the strip is clearly observed at 160 and 220 GHz for the large and small antennas, respectively. As expected, the resonant frequency increased as the lateral dimensions decreased in a similar manner to the case for standard diabolo antennas. The peak values at 160 and 220 GHz were 0.26 and 0.20 A/m, which corresponded to enhancement factors of 96 and 74, respectively. The full width at half maximum (FWHM) values were 30 and 40 GHz, respectively. These narrow frequency bands inevitably originate from the resonant properties of diabolo antennas, in which the strip and fins are involved in inductance and capacitance in the equivalent circuit model.

Next, the respective single U-shaped diabolo antennas are nested to form nested U-shaped antennas, shown in Fig. 1(c). The gap between the respective antennas was fixed at 15 μm. Metallic planar structures with a resolution of 10 μm can be easily fabricated using the standard photolithography process. It should be noted that U-shaped diabolo antennas consisting of rectangular fins are more suitable for nested geometry compared to the standard diabolo antennas with triangular fins. Figure 1(e) shows the frequency responses of the nested U-shaped antenna. A probe port is configured on the strip of the outer antenna (probe 1) and another on the inner antenna (probe 2). As clearly seen in the figure, probe 1 shows a single peak response, similar to that of the large single U-shaped antenna mentioned above. Compared to the single U-shaped antenna, the resonance frequency slightly decreased from 160 to 147 GHz, and the resonance became sharper. On the other hand, probe 2 shows a double peak structure at 147 and 204 GHz. The resonance peak at 147 GHz can be attributed to the resonance of the outer antenna. Therefore, the present result indicates that the behavior of the inner antenna is strongly influenced by the outer antenna, leading to the double peak structure. The frequency range exceeding the half maximum was 95 GHz, which is more than twice as wide as that of the single U-shaped antenna.

This behavior is clearly seen in the density plot of the horizontal component of the oscillating magnetic field at 147 and 204 GHz, as shown in Fig. 2. The results for two different probe heights (z=10 and 3000 nm) are shown. Strong enhancement is observed only on the strips, while the enhancement at the gap is negligible. It should be noted that the enhancement on the inner strip was also obtained at 147 GHz corresponding to the resonance of the outer antenna, though it is weaker than on the outer strip. On the other hand, the enhancement at 204 GHz was observed only in the inner strip. This asymmetric behavior resulted in the broadband enhancement of the oscillating magnetic fields at probe 2 on the inner strip.

Optics EXPRESS

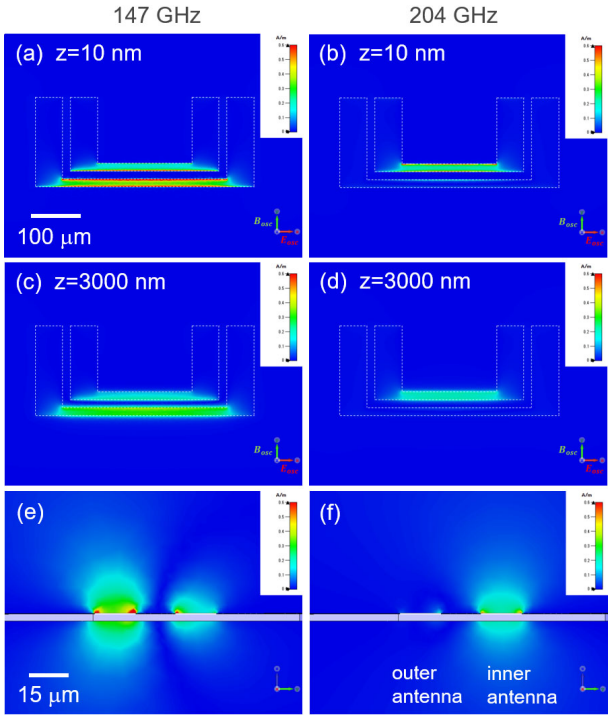

Fig. 2. Density plots of the horizontal component of oscillating magnetic field at 147 GHz (a), (c), (e) and 204 GHz (b), (d), (f). The probe height within the *xy* plane was z=10 nm (a), (b), and z=3000 nm (c), (d). White dotted lines indicate the antenna shape. Density plots within the *yz* plane (x = 0 nm at the antenna center) were shown in (e) and (f).

The enhancement factor at z=10 nm was found to be 132 at 147 GHz for probe 1; for probe 2, it was 67 and 80 at 147 and 204 GHz, respectively. The enhancement factor gradually decreased with increasing probe height, but its lateral distribution was almost unchanged, as shown by the simulation results at z=10 and 3000 nm. The vertical dependence of the oscillating magnetic field component is depicted within the *yz* plane containing the probes 1 and 2 (Figs. 2(e) and (f)). For probe 1 , the enhanced region at 147 GHz was extended far above the strip surface, and the enhancement factor was still 106 and 73 at z=5 and 10 μm, respectively; for probe 2, it was 53 and 32 at z=5 and 10 μm, respectively. Besides, the enhancement factor at 204 GHz was 67 and 49 at z=5 and 10 μm for probe 2, respectively. These long-range enhancement factors in the vertical direction is qualitatively understandable according to the Ampère's circuital law. From the practical viewpoint, the transition probability of the magnetic dipole transition is proportional to the square of the oscillating magnetic field component. Thus, the present antennas are useful to enhance the broadband sensitivity of ESR measurements not only for thin film samples but also for bulky samples with dimensions on the order of the strip width.

In order to understand the origin of the broadband enhancement, the horizontal components of oscillating electric field and surface current density were shown in Fig. 3. It is clearly seen that the lateral electric field component at 147 GHz was strongly enhanced between the gaps at the fin part, compared to the case for 204 GHz. This result indicates a capacitive coupling between the inner and outer antennas, resulting in circulating currents flowing in both antennas. Indeed, surface current densities at 147 GHz were finite on both strips and flowed in opposite directions each other, as shown in Fig. 3(c). This fact accounts for the field enhancement of the inner antenna strip at 147 GHz. On the other hand, such a couped behavior was not observed

Optics EXPRESS

at 204 GHz. So, the surface current resonantly flowed back and forth in the strip of the inner antenna, as shown in Fig. 3(d). It was found that the high-permittivity dielectric substrate played an essential role in this coupled behavior as the coupling was substantially weakened for nested U-shaped antennas without the substrate.

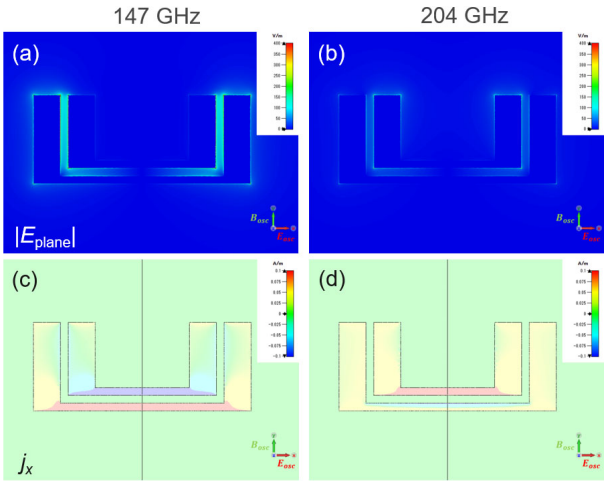

Fig. 3. Density plot of the horizontal component of oscillating electric field (a), (b), and surface current density (c), (d).

Generally speaking, the resonance width $\Delta f = f_0/Q$ depends on losses accompanied with antennas, where f_0 and Q are the resonance frequency and the quality factor, respectively. The quality factor is known to be decomposed into dielectric, conductive, and radiative losses of the antenna, and is given by $1/Q = 1/Q_{\text{diele}} + 1/Q_{\text{cond}} + 1/Q_{\text{rad}}$. Therefore, the most lossy term (namely, the smallest Q term) plays the dominant role in the resonance width. To clarify this, we performed simulations of the antennas made of different materials and of the antenna without the dielectric substrate. It was found that either antenna material or substrate has only a small contribution to the antenna loss (see Supplement 1). Therefore, radiative losses are supposed to be responsible for the resonance width of the nested U-shaped antenna, similar to the cases for other nanoantennas [14]. From this analysis, the spectral narrowing of the nested U-shaped antenna at 147 GHz, shown in Fig. 1(e), can be understood in terms of the above-mentioned coupled behavior of the inner and outer antennas, in which more energy density is stored within the nested regions, compared to the single U-shaped antenna. Similar narrowing effect in the frequency response was previously reported in vertically coupled diabolo antennas [14].

Figure 4 shows the dependence of the antenna height h on the frequency response of the nested U-shaped antennas for w=(a) 252 μm, (b) 282 μm, (c) 378 μm, and (d) 419 μm. It is clearly seen that the frequency band monotonously extends and the peak height decreases as the antenna height is reduced. In addition, an increase in the antenna width w leads to reduction in the frequency band. For the case of w=252 μm and h=146 μm, shown in Fig. 4(a), the frequency band with an enhancement factor exceeding 10 ranges between 200 and 450 GHz. So, the frequency band of Δf ~250 GHz was achieved.

Figure 5 shows the broadband frequency response of the nested U-shaped antennas for w=252 μm and h=146 μm. It is noteworthy that a broad enhancement (~7) was also observed in the frequency range of 700 to 950 GHz, in addition to the enhancement between 200 and 400 GHz. This behavior can be attributed to the third harmonics components. Considering the boundary conditions, the amplitude of the second harmonic components should be zero at the center of the strip, while that of the third harmonics components can be finite. Indeed, the outer strip was

Optics EXPRESS

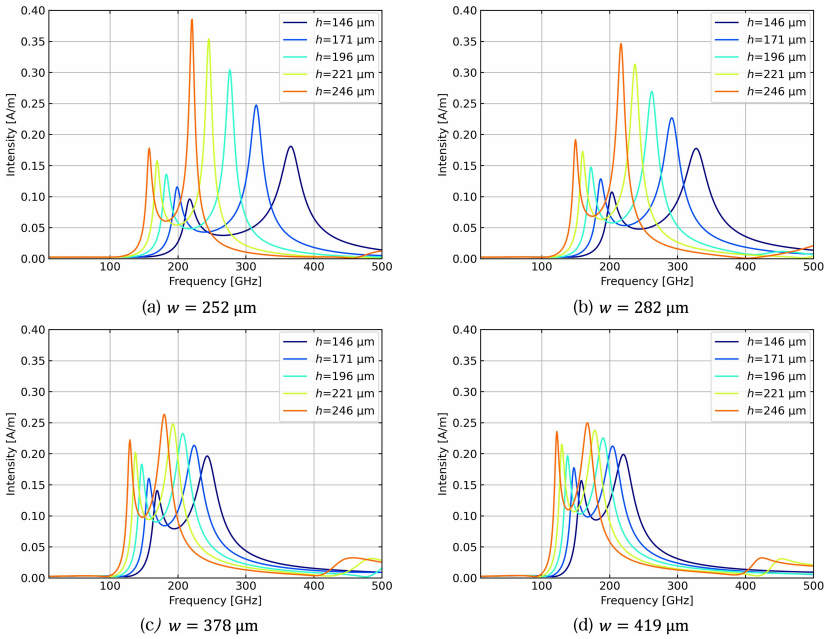

Fig. 4. Variations of the frequency response of the nested U-shaped antennas as a function of antenna height h. (a) w=252 μm, (b) w=282 μm, (c) w=378 μm, and (d) w=419 μm.

separated into three field-enhanced regions by a line node, and a substantial enhancement at 839 GHz was obtained at the center of the inner strip, as shown in the inset.

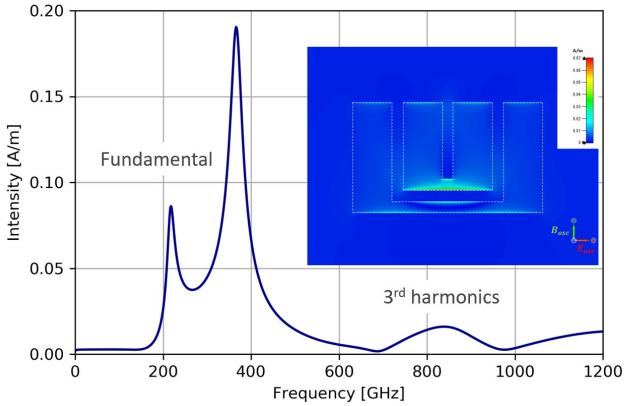

Fig. 5. Broadband frequency response of the nested U-shaped antenna for the case of w=252 μm and h=146 μm. The inset shows the density plot of the horizontal component of the oscillating magnetic field at 839 GHz.

According to the ESR condition $h\nu = g\mu_B B$, where h is the Planck constant, ν is the frequency of the electromagnetic wave, g is the g factor, μ_B is the Bohr magneton, and B is the applied magnetic flux density, the resonant frequency of 450 GHz corresponds to the resonance field of 16 T for g=2, a typical magnetic field that can be generated by conventional superconducting magnets. Therefore, the above-mentioned frequency range is broad enough to enhance the sensitivity of high-frequency ESR measurement. It is noted that the working frequency band has

Optics EXPRESS

no upper limit because the resonant frequency can be increased by reducing the antenna size. Indeed, diabolo antennas are shown to work even in the optical range [20,22]. So, by adjusting the geometrical parameters, the working frequency band can be tuned beyond 1 THz. Such high-frequency AFMR modes have been indeed observed at 1.1 THz in a typical antiferromagnet NiO at room temperature [23].

Figure 6 shows the frequency response of the oscillating magnetic field component for a triply nested U-shaped antenna in the frequency range up to 500 GHz. Three probe ports were configured at the center of the outer, middle, and inner strips. Probe 1 showed a sharp peak at around 129 GHz, and its intensity was 0.49 A/m. On the other hand, probe 2 showed double peaks at 129 and 168 GHz. As mentioned in Figs. 1(d) and (e), the peak at 129 GHz originated from a contribution of the outermost antenna. Finally, probe 3 also showed a double peak at 168 and 257 GHz, the former of which originated from a contribution of the middle antenna, similar to the peak at 129 GHz of probe 2. These results indicate that the intensity of the oscillating magnetic field of a certain antenna is given by the sum of the contributions from the antenna itself and the outer neighboring antenna. The contributions from the second outer neighboring antenna seems to be small, judging from the small peak at 129 GHz of probe 3. Thus, doubly nested U-shaped antennas are found to be enough for broadband enhancement at a single probe site.

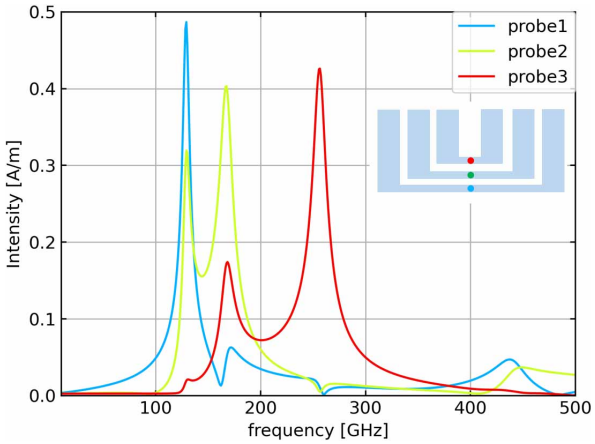

Fig. 6. Frequency responses of the triply nested U-shaped antenna measured at different probe ports. The inset shows the antenna shape and the probe positions.

In the practical experimental setup, nested U-shaped antennas will be combined with the mechanically detected ESR apparatus developed by our group [24,25]. In this technique, a tiny sample is mounted on a thin membrane, and a magnetic field is swept under the irradiation of sub-THz waves. Then, the sample magnetization $M = \mu_B(N_{down} - N_{up})$ changes at the ESR transition, where N_{down} and N_{up} are the numbers of down and up spin states, respectively. This process, in turn, exerts a change in magnetic torque or magnetic gradient force on the sample, resulting in an ESR-induced deformation of the membrane. The deformation could be sensitively detected either optically [26] or electrically [27]. Typically, the membrane and sample dimensions were on the order of 1 and 0.1 mm, respectively. So, most of the incident sub-THz waves transmitted through the membrane without interacting with the sample in the previous setup. By fabricating a nested U-shaped antenna on the membrane, sub-THz waves are efficiently gathered by the antenna and can be focused onto the sample placed at the strip. Since the lateral dimensions of the nested U-shaped antenna are several hundreds of μm in the frequency range of interest, as shown in Fig. 4, the antenna nicely fits the membrane diameter. Accordingly, broadband sensitivity enhancement is expected using nested U-shaped antennas without any

Optics EXPRESS

other modifications of the existing setup. Experimental attempts are currently ongoing to validate the simulation results shown above.

4. Conclusion

In this study, we numerically investigate the geometrical dependence of modified diabolo antennas or nested U-shaped antennas for broadband enhancement of sub-THz oscillating magnetic fields. According to the systematic simulation results, the nested geometry produced a double-peak enhancement at the inner antenna, and its enhancement factor reached 100, depending on the geometrical parameters. Thus, mounting a sample on the inner antenna strip will generate enhanced oscillating magnetic fields at the sample position, leading to substantial sensitivity improvement in high-frequency ESR measurement. Since the present technique does not entail any other modification of the existing setup, it will be useful for enhancing the local magnetic interactions in the broad sub-THz region.

Funding. Japan Society for the Promotion of Science (JP21H01040); Nippon Sheet Glass Foundation for Materials Science and Engineering; Casio Science Promotion Foundation.

Acknowledgments. The authors acknowledge H. Takahashi and Y. Shoji for their technical assistance.

Disclosures. The authors declare no conflicts of interest.

Data availability. Data underlying the results presented in this paper are not publicly available at this time but may be obtained from the authors upon reasonable request.

Supplemental document. See Supplement 1 for supporting content.

References

1. Z. N. Chen and M. Y. W. Chia, *Broadband Planar Antennas: Design and Applications* (John Wiley & Sons, 2006), Chap. 2.
2. K. Crozier, A. Sundaramurthy, G. Kino, *et al.*, "Optical antennas: resonators for local field enhancement," J. Appl. Phys. **94**(7), 4632–4642 (2003).
3. M. Agio and A. Alù, eds., *Optical Antennas* (Cambridge University Press, 2013), Chap. 5.
4. S. Dodson, M. Haggui, R. Bachelot, *et al.*, "Optimizing electromagnetic hotspots in plasmonic bowtie nanoantennae," J. Phys. Chem. Lett. **4**(3), 496–501 (2013).
5. A. Kinkhabwala, Z. Yu, S. Fan, *et al.*, "Large single-molecule fluorescence enhancements produced by a bowtie nanoantenna," Nat. Photonics **3**(11), 654–657 (2009).
6. S. Sederberg and A. Elezzabi, "Nanoscale plasmonic contour bowtie antenna operating in the mid-infrared," Opt. Express **19**(16), 15532–15537 (2011).
7. J. Olson, S. Dominguez-Medina, A. Hoggard, *et al.*, "Optical characterization of single plasmonic nanoparticles," Chem. Soc. Rev. **44**(1), 40–57 (2015).
8. X. Lu, M. Rycenga, S. E. Skrabalak, *et al.*, "Chemical synthesis of novel plasmonic nanoparticles," Annu. Rev. Phys. Chem. **60**(1), 167–192 (2009).
9. P. Verma, "Tip-enhanced raman spectroscopy: technique and recent advances," Chem. Rev. **117**(9), 6447–6466 (2017).
10. T. Deckert-Gaudig, A. Taguchi, S. Kawata, *et al.*, "Tip-enhanced raman spectroscopy–from early developments to recent advances," Chem. Soc. Rev. **46**(13), 4077–4110 (2017).
11. M. A. Santiago-Cordoba, S. V. Boriskina, F. Vollmer, *et al.*, "Nanoparticle-based protein detection by optical shift of a resonant microcavity," Appl. Phys. Lett. **99**(7), 073701 (2011).
12. D. Yu, M. Humar, K. Meserve, *et al.*, "Whispering-gallery-mode sensors for biological and physical sensing," Nat. Rev. Methods Primers **1**(1), 83 (2021).
13. D. G. Baranov, R. S. Savelev, S. V. Li, *et al.*, "Modifying magnetic dipole spontaneous emission with nanophotonic structures," Laser Photonics Rev. **11**(3), 1600268 (2017).
14. M. Mivelle, T. Grosjean, G. W. Burr, *et al.*, "Strong modification of magnetic dipole emission through diabolo nanoantennas," ACS Photonics **2**(8), 1071–1076 (2015).
15. L. Tesi, D. Bloos, M. Hrtoň, *et al.*, "Plasmonic metasurface resonators to enhance terahertz magnetic fields for high-frequency electron paramagnetic resonance," Small Methods **5**(9), 2100376 (2021).
16. N. Dayan, Y. Ishay, Y. Artzi, *et al.*, "Advanced surface resonators for electron spin resonance of single microcrystals," Rev. Sci. Instrum. **89**(12), 124707 (2018).
17. T. Jungwirth, X. Marti, P. Wadley, *et al.*, "Antiferromagnetic spintronics," Nat. Nanotechnol. **11**(3), 231–241 (2016).
18. V. Baltz, A. Manchon, M. Tsoi, *et al.*, "Antiferromagnetic spintronics," Rev. Mod. Phys. **90**(1), 015005 (2018).
19. S. M. Rezende, A. Azevedo, and R. L. Rodríguez-Suárez, "Introduction to antiferromagnetic magnons," J. Appl. Phys. **126**(15), 151101 (2019).

Optics EXPRESS

20. T. Grosjean, M. Mivelle, F. Baida, *et al.*, "Diabolo nanoantenna for enhancing and confining the magnetic optical field," Nano Lett. **11**(3), 1009–1013 (2011).
21. X.-D. Chen, E.-H. Wang, L.-K. Shan, *et al.*, "Focusing the electromagnetic field to $10^{-6}\lambda$ for ultra-high enhancement of field-matter interaction," Nat. Commun. **12**(1), 6389 (2021).
22. H. Guo, B. Simpkins, J. D. Caldwell, *et al.*, "Resonance spectra of diabolo optical antenna arrays," AIP Adv. **5**(10), 107149 (2015).
23. E. Ohmichi, Y. Shoji, H. Takahashi, *et al.*, "Frequency-domain antiferromagnetic resonance spectroscopy of nio," J. Phys. Soc. Jpn. **91**(9), 095001 (2022).
24. H. Takahashi, K. Ishimura, T. Okamoto, *et al.*, "Note: Force-and torque-detection of high frequency electron spin resonance using a membrane-type surface-stress sensor," Rev. Sci. Instrum. **89**(3), 036108 (2018).
25. H. Takahashi, T. Okamoto, K. Ishimura, *et al.*, "Force-detected high-frequency electron spin resonance spectroscopy using magnet-mounted nanomembrane: Robust detection of thermal magnetization modulation," Rev. Sci. Instrum. **89**(8), 083905 (2018).
26. E. Ohmichi, Y. Tokuda, R. Tabuse, *et al.*, "Multi-frequency force-detected electron spin resonance in the millimeter-wave region up to 150 ghz," Rev. Sci. Instrum. **87**(7), 073904 (2016).
27. H. Takahashi, K. Ishimura, T. Okamoto, *et al.*, "New method for torque magnetometry using a commercially available membrane-type surface stress sensor," J. Phys. Soc. Jpn. **86**(6), 063002 (2017).